

# Efficiency Analysis of a Bi-directional DC/DC Converter for Wireless Energy Transfer Applications

Erdem Asa<sup>1</sup>, Kerim Colak<sup>2</sup>, Dariusz Czarkowski<sup>1</sup>, Bunyamin Tamyurek<sup>3</sup>

<sup>1</sup>New York University, Polytechnic School of Engineering, New York, USA

<sup>2</sup>Istanbul Ulasim A.S., Istanbul, Turkey

<sup>3</sup>Eskisehir Osmangazi University, Electrical & Electronics Engineering, Eskisehir, Turkey

**Abstract—**In this study, analysis of a bi-directional half-bridge inverter for wireless power transfer applications is realized. The presented converter topology is explored to reveal the maximum efficiency points with a variable phase shift function between the dual active bridge (DAB) switches. The examination of the converter is provided in terms of variable load and coupling co-efficient factor at a constant switching frequency. A 1 kW contactless system is designed with an output of 100 V by testing the different load conditions at an 8 inch gap between coils. Experimental results indicate that the demonstrated system, which has an average efficiency improvement of 2% with an optimized phase shift between switches, offers higher efficiency in comparison to conventional topologies.

**Keywords**—asymmetrical inverter, bi-directional, dual active bridge, phase-shift, resonant converter, wireless energy

## I. INTRODUCTION

Due to an increase of battery powered applications, inductive power transfer (IPT) is a growing technology to supply power to a variety of implementation from smartphone charging platforms, medical implant devices to electric vehicle charging [1]-[4]. The IPT increases the system flexibility and equipment safety with the elimination of a physical electrical contact [5]-[7]. Bi-directional IPT system is very suitable for active loads, regenerative energy capability, and efficiency improvement [8]-[9] as discussed in the paper. A conventional bi-directional IPT system is demonstrated in Fig. 1. As seen in the figure, the system has a symmetrical structure and consists of two main stages: the primary and secondary platforms. The secondary side load is represented as a voltage source that can be a battery pack used for retrieving or storing energy.

The bi-directional IPT system must be well designed and organized in order to achieve high efficiency [10]. Several bi-directional circuit topologies, control algorithms, and compensation strategies are carried out in the literature [11]-[20]. A series, parallel, series-parallel, and LCL compensation networks have been analyzed with different control methods for bi-directional wireless applications in [11]-[14]. A steady state model of bi-directional IPT has been presented to show

the system performances in [15]-[16]. A power flow management with proportional integral (PI) and proportional integral derivative (PID) modulations has been implemented between load and grid in [17]. Researchers in [18] have explored bi-directional IPT system for multiple pickups to integrate low power modules into the high power demands. A current sourced IPT bi-directional system has been investigated between the grid and several individual connected loads in [19]-[20]. However, all mentioned papers above consider a full-bridge inverter topology on both side primary and secondary platforms. Furthermore, efficiency analysis has not been revealed deeply attentive for bi-directional systems.

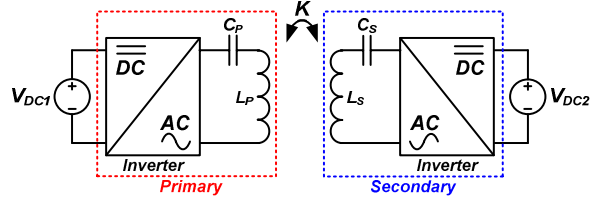


Fig. 1. An illustration of a bi-directional inductive coupling transfer (IPT) system.

In this paper, a half-bridge inverter is studied for bi-directional IPT systems. A phase shifted modulation technique is used between primary and secondary inverter ports in order to obtain maximum efficiency points. The topology is explored with different load conditions at the constant frequency and constant output voltage. The converter model controllability is analyzed and the transfer function of the converter is derived. The system performance is confirmed with experimental results at 8 inch air gaps in coreless transformer, 150 kHz operating frequency, and a 1 kW load with a maximum efficiency of 91% in laboratory conditions.

## II. CIRCUIT ANALYSIS OF THE WIRELESS POWER LINK

The investigated phase shift principle of a bi-directional IPT circuit topology for the wireless power transfer is shown in Fig. 2. It comprises two half bridge resonant inverters in the primary and secondary side, an air gap coreless transformer,

and resonant capacitors in each platform. The constant output voltage of the system is managed by an asymmetrical duty cycle control and the phase-shift angle of the transistors between inverter ports manages the efficiency optimization in order to reduce switching losses in the system.

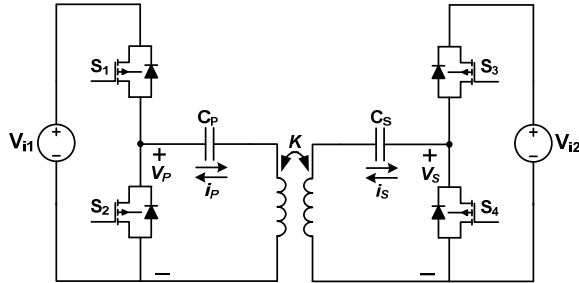


Fig. 2. The analyzed bi-directional IPT system.

In order to perform the circuit analysis, the wireless power link can be represented as two coupled inductors and two resonant capacitors connected in series as shown in Fig. 3(a). In this model, the voltage sources are  $V_{i1}$  and  $V_{i2}$ , two coupled inductors are  $L_P$  and  $L_S$  with equivalent series resistances  $R_P$  and  $R_S$ .  $K$  is a coupling factor between the two coils and  $C_P$  and  $C_S$  are resonant capacitors. The two coupled inductors can be equivalently modeled as a transformer with proper leakage and magnetizing inductances.

To simplify analysis, both coils  $L_P$  and  $L_S$  are assumed to be identical and equal to  $L$ . Then, the model can be equivalently represented by the circuit in Fig. 3(b). In this model  $V_{P,1}$  and  $V_{S,1}$  are fundamental component of voltage sources  $V_P$  and  $V_S$ , respectively.  $Z_{P,eq}$  and  $Z_{S,eq}$  are equivalent values where  $Z_{P,eq} = \{1/j\omega C_P + j\omega L + R_P\}$ ,  $Z_{S,eq} = \{1/j\omega C_S + j\omega L + R_S\}$ .  $Z_M$  is the magnetizing impedance related to the coupled inductors by  $Z_M = j\omega L_M$ .

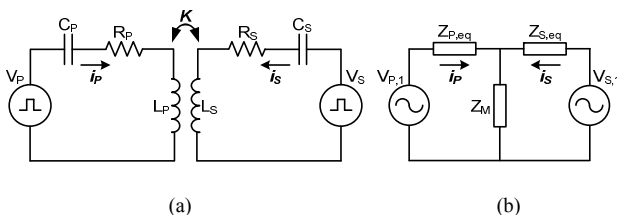


Fig. 3. Schematics of wireless power link (a) equivalent circuit model, (b) simplified model.

The model of Fig. 3(b) is related to the model of Fig. 3(a) by the following equations.

$$\begin{aligned} L_M &= K\sqrt{L_P L_S} = KL \\ L_L &= L - L_M = (1 - K)L \end{aligned} \quad (1)$$

The primary resonant tank square wave voltage  $v_P$  and the secondary resonant tank square wave voltage  $v_S$  are positive or

negative during the different cycles. Thus,  $v_P(t)$  and  $v_S(t)$  can be stated considering the duty cycle  $D_P$ ,  $D_S$ , and phase shift angle  $\phi$  between the inverter ports as

$$v_P(t) = \begin{cases} V_{i1}, & 0 < t \leq D_P T \\ 0, & D_P T < t \leq T \end{cases} \quad (2)$$

and

$$v_S(t) = \begin{cases} V_{i2}, & -\phi T/(2\pi) < t \leq -\phi T/(2\pi) + D_S T \\ 0, & D_S T < t \leq T \end{cases} \quad (3)$$

The fundamental components of the voltages  $v_{P,1}(t)$  and  $v_{P,2}(t)$  can be stated with the duty cycle phase angles  $\theta_P$ ,  $\theta_S$  in the phasor domain as

$$V_{P,1} = V_{Pm} e^{j(\theta_P)} \quad (4)$$

$$V_{S,1} = V_{Sm} e^{j(\theta_S + \phi)} \quad (5)$$

The amplitude of the real voltage of the fundamental component of  $V_{P,1}$  and  $V_{S,1}$  can be derived with the duty cycle ratio  $D$  using Fundamental Harmonic Approximation (FHA) as

$$V_{P,1} = \frac{2V_{i1}}{\pi} \sin(\pi D_P) e^{j(\theta_P)} \quad (6)$$

$$V_{S,1} = \frac{2V_{i2}}{\pi} \sin(\pi D_S) e^{j(\theta_S + \phi)} \quad (7)$$

where  $D_P$  and  $D_S$  are duty cycle values in each inverter port, respectively.  $\theta_P$  and  $\theta_S$  are given by the following equations

$$\theta_P = \tan^{-1} \left[ \frac{\sin(2\pi D_P)}{1 - \cos(2\pi D_P)} \right] \quad (8)$$

$$\theta_S = \tan^{-1} \left[ \frac{\sin(2\pi D_S)}{1 - \cos(2\pi D_S)} \right] \quad (9)$$

Using the Kirchhoff's voltage law, primary and secondary resonant tank in a matrix form is

$$\begin{bmatrix} V_{P,1} \\ V_{S,1} \end{bmatrix} = \begin{bmatrix} \frac{1}{j\omega C_P} + j\omega L_P + R_P & j\omega L_M \\ j\omega L_M & \frac{1}{j\omega C_S} + j\omega L_S + R_S \end{bmatrix} \begin{bmatrix} I_P \\ I_S \end{bmatrix} \quad (10)$$

If the system is operated at the resonant frequency  $\omega_R$  as

$$\omega_R = \frac{1}{\sqrt{L_P C_P}} = \frac{1}{\sqrt{L_S C_S}} \quad (11)$$

The corresponding fundamental currents of the contactless system in the primary and secondary winding can be written as

$$I_P = \frac{V_{P,1} R_S - V_{S,1} (j\omega L_M)}{R_P R_S + (\omega L_M)^2} \quad (12)$$

$$I_S = \frac{V_{S,1}R_P - V_{P,1}(j\omega L_M)}{R_P R_S + (\omega L_M)^2} \quad (13)$$

Normalized parameters help to find the transfer function of the system using design parameter values. These equations are defined and explained as follows.

$$Z_O = \sqrt{\frac{L_P}{C_P}}, \quad \omega_N = \frac{\omega_{sw}}{\omega_R} \quad (14)$$

Characteristic impedance  $Z_O$  affects the operating frequency range of the system. The normalized frequency  $\omega_N$  depends on the switching  $\omega_{sw}$  and resonant frequency  $\omega_R$ . The voltage and current transfer functions of the system is deduced as

$$|M_V| = \left| \frac{V_{S,1}}{V_{P,1}} \right| = \left| \frac{\frac{2V_S}{\pi} \sin(\pi D_S) e^{j(\theta_S + \phi)}}{\frac{2V_P}{\pi} \sin(\pi D_P) e^{j(\theta_P)}} \right| \quad (15)$$

$$|M_I| = \left| \frac{I_S}{I_P} \right| = \left| \frac{V_{S,1}R_P - V_{P,1}(j\omega L_M)}{V_{P,1}R_S - V_{S,1}(j\omega L_M)} \right| \quad (16)$$

### III. THE POWER FLOW ANALYSIS

Active and reactive power flow of a bi-directional contactless system can be simplified with the amplitude of the primary voltage with a function of the primary current, and the secondary voltage with a function of the secondary current as shown in Fig. 4.

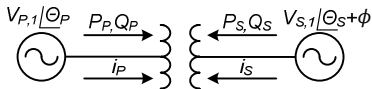


Fig. 4. A simplified power flow chart between inverter parts.

As seen in the figure, if the equivalent impedance, voltage amplitude and phases can be regulated, the effective power flow management would be implemented. The active  $P_P$ ,  $P_S$  and reactive powers  $Q_P$ ,  $Q_S$  can be obtained with the mathematical calculation for the primary and secondary side as

$$P_P = Re \left\{ \frac{V_{P,1}I_P^*}{2} \right\} \quad (17)$$

$$= \frac{V_{Pm}^2 R_S}{2[R_P R_S + (\omega L_M)^2]} + \frac{V_{Pm} V_{Sm} \omega L_M}{2[R_P R_S + (\omega L_M)^2]} \sin(\theta_S - \theta_P + \phi) \quad (18)$$

$$P_S = Re \left\{ \frac{V_{S,1}I_S^*}{2} \right\} \quad (19)$$

$$= \frac{V_{Sm}^2 R_P}{2[R_P R_S + (\omega L_M)^2]} - \frac{V_{Pm} V_{Sm} \omega L_M}{2[R_P R_S + (\omega L_M)^2]} \sin(\theta_S - \theta_P + \phi) \quad (20)$$

$$Q_P = Im \left\{ \frac{V_{P,1}I_P^*}{2} \right\} \quad (21)$$

$$= \frac{V_{Pm} V_{Sm} \omega L_M}{2[R_P R_S + (\omega L_M)^2]} \cos(\theta_S - \theta_P + \phi) \quad (22)$$

$$Q_S = Im \left\{ \frac{V_{S,1}I_S^*}{2} \right\} \quad (23)$$

$$Q_S = \frac{V_{Pm} V_{Sm} \omega L_M}{2[R_P R_S + (\omega L_M)^2]} \cos(\theta_S - \theta_P + \phi) \quad (24)$$

By changing the phase difference between ports and duty ratio in each inverter, the power flow between sources can be controlled. For the two unbalanced input voltage combinations, the power flow is analyzed in Fig. 5. The phase shift from  $-180^\circ$  to  $180^\circ$  obtains the phase difference in each port sequentially. The function of phase sliding shows that the input power at various angles is controlled by the duty cycle in every single port.

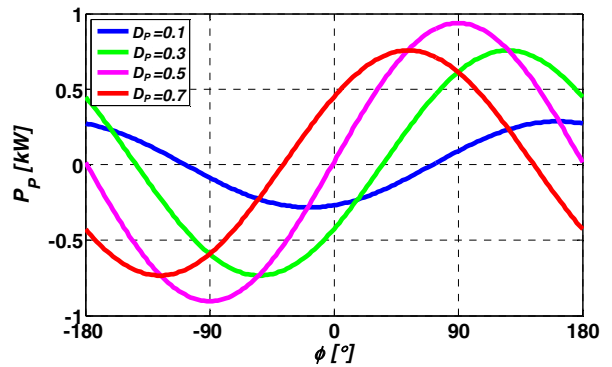


Fig. 5. The input power range with two unbalanced sources with phase shift angle and duty cycle ratio.

### IV. EFFICIENCY ANALYSIS OF THE SYSTEM

The system efficiency can be described as two different conditions; when the primary side supplies the power to the secondary side, and the power from the secondary side is supplied to the primary side. If  $\theta_S - \theta_P + \phi = 90^\circ$ , the power is delivered from the primary side to the secondary side. The efficiency of the system can be written from the primary side as

$$\eta_P = \left| \frac{P_S}{P_P} \right| = \frac{V_{Sm} V_{Pm} \omega L_M - V_{Sm}^2 R_P}{V_{Pm} V_{Sm} \omega L_M + V_{Pm}^2 R_S} \quad (25)$$

If  $\theta_S - \theta_P + \phi = -90^\circ$ , the power is provided from the secondary side to the primary side. From the secondary side, the system efficiency can be defined as

$$\eta_S = \left| \frac{P_P}{P_S} \right| = \frac{V_{Pm} V_{Sm} \omega L_M - V_{Pm}^2 R_S}{V_{Sm} V_{Pm} \omega L_M + V_{Sm}^2 R_P} \quad (26)$$

The efficiency functions can be also written as

$$\eta_P = \frac{\omega L_M - \frac{V_{Sm}}{V_{Pm}} R_P}{\omega L_M + \frac{V_{Pm}}{V_{Sm}} R_S} \quad (27)$$

$$\eta_S = \frac{\omega L_M - (\frac{V_{Pm}}{V_{Sm}}) R_S}{\omega L_M + (\frac{V_{Sm}}{V_{Pm}}) R_P} \quad (28)$$

In order to find the maximum efficiency points, efficiency functions can be differentiated with respect to  $(\frac{V_{Sm}}{V_{Pm}})$ .

$$\frac{d\eta_P}{d(\frac{V_{Sm}}{V_{Pm}})} = 0, \quad \frac{d\eta_S}{d(\frac{V_{Sm}}{V_{Pm}})} = 0 \quad (29)$$

(29) can be solved as

$$-R_P \omega L_M \left( \frac{V_{Sm}}{V_{Pm}} \right)^2 - 2R_P R_S \cdot \left( \frac{V_{Sm}}{V_{Pm}} \right) + R_S \omega L_M = 0 \quad (30)$$

Assuming that  $\omega L_M \gg R_P$  and  $\omega L_M \gg R_S$ , maximum efficiency point can be found as

$$\frac{V_{Sm}}{V_{Pm}} = \sqrt{\frac{R_S}{R_P}} \quad (31)$$

Using (8) and (9), the duty ratio phases in each port as

$$\theta_P = \frac{\pi}{2} - \pi D_P \quad (32)$$

$$\theta_S = \frac{\pi}{2} - \pi D_S \quad (33)$$

The optimal phase shift function between primary and secondary side inverter ports are given by using the maximum efficiency points in forward direction,

$$\phi = 90^\circ - \theta_S + \theta_P \quad (34)$$

and in reverse direction as

$$\phi = -90^\circ - \theta_S + \theta_P \quad (35)$$

The highest efficiency is achieved when the sinus function is  $90^\circ$ . In order to eliminate reflected reactive power from both sides, the phase shift function should be in the boundary

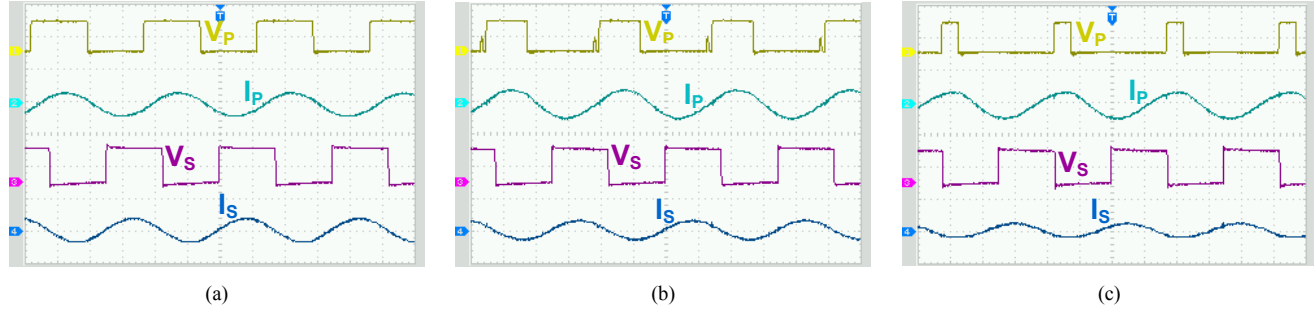


Fig. 6. The converter primary resonant tank voltage  $V_p$ , current  $I_p$  and secondary resonant tank voltage  $V_s$ , current  $I_s$  waveforms for  $V_p$  (100 V/div),  $I_p$  (10 A/div),  $V_s$  (100 V/div),  $I_s$  (20 A/div), a)  $D_p=0.5, D_s=0.5, \phi=142^\circ, 900$  W, b)  $D_p=0.41, D_s=0.5, \phi=152^\circ, 600$  W, c)  $D_p=0.2, D_s=0.5, \phi=164^\circ, 300$  W.

condition considering the different load and duty cycle conditions with described functions above.

## V. EXPERIMENTAL RESULTS

The proposed bi-directional wireless system is designed for 1 kW, 120 V input voltage, and 100 V output voltage rating as a laboratory prototype. The coreless transformer is tested with 8 inch distances between coils which results in 0.25 coupling factor. The topology parameters of the converter are given in Table I.

TABLE I

Symbol	Parameter	Value
$V_i$	dc input voltage	120 V
$V_o$	dc output voltage range	100 V
$I_o$	dc output current	10 A
$P_o$	maximum output power	1 kW
$C_p, C_s$	resonant capacitors	40 nF
$L_p, L_s$	coil self-inductances	25 uH
$d$	square coil dimension	2.5 x 2.5 feet
$n$	coil turn number	4
$f_{sw}$	operating frequency	150 kHz

The characteristic waveforms of the proposed converter described in section III and IV are given to verify circuit operation. With the optimized phase shift angle between primary and secondary side, the selected current and voltage waveforms at different power range are given in Fig. 6. Here, the output voltage is set at 100 V and managed by asymmetrical duty-cycle control.

The efficiency comparison of the proposed topology with the normal half bridge rectifier system is given in Fig. 7. The efficiency of the converter is always greater than normal half bridge rectifier in all different output power conditions with the optimized phase shift function. The proposed analysis improves the system efficiency 2% overall. The system reaches the maximum efficiency 91% around 700 W with the phase shift angle at 160 degrees.

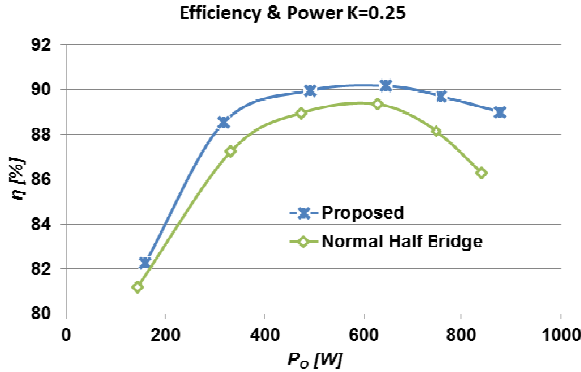


Fig. 7. The efficiency results of the bi-directional converters.

## VI. CONCLUSIONS

In this study, a phase shift optimization of a bi-directional half bridge converter is presented for wireless power transfer applications. The system analysis reveals the maximum efficiency points with the optimal phase shift between inverter ports. The system model analysis with the circuit description is given considering primary and secondary side power flow in a both direction. The transfer function of the converter is derived analytically. The output of the system is adjusted by the asymmetrical duty cycle control. The system performance is confirmed with theoretical and experimental results at various loads at a constant coupling factor. To verify the proposed optimized phase shifted bi-directional inverter, a 1 kW prototype is designed at 120 V input. The laboratory prototype achieved a 91% maximum efficiency.

## REFERENCES

- [1] K. Colak, E. Asa, M. Bojarski, D. Czarkowski, O. C. Onar, "A Novel Phase Shift Control of Semi-Bridgeless Active Rectifier for Wireless Power Transfer" IEEE Transaction on Power Electronics, vol.30, no.11, pp.6288-6297, Nov. 2015.
- [2] O. Knecht, R. Bosshard, J. Kolar, "High Efficiency Transcutaneous Energy Transfer for Implantable Mechanical Heart Support Systems," IEEE Transactions on Power Electronics, vol.30, no.11, pp.6221-6236, Nov. 2015.
- [3] E. Asa, K. Colak, M. Bojarski, D. Czarkowski, "A Novel Multi-Level Phase-Controlled Resonant Inverter with Common Mode Capacitor for Wireless EV Chargers," IEEE International Conference on Transportation Electrification (ITEC), pp.1-6, Jun. 2015.
- [4] M. Nalbant, "Wireless Power Transmitter Having Low Noise and High Efficiency, and Related Methods," U.S. Patent, 2014/0132077 A1 May 15, 2014.
- [5] E. Asa, K. Colak, M. Bojarski, D. Czarkowski, "A Novel Phase Control of Semi Bridgeless Active Rectifier for Wireless Power Transfer Applications," IEEE Applied Power Electronics Conference and Exposition (APEC), pp.3225-3231, Mar. 2015.
- [6] R. Ramzan, F. Zafar, "High-Efficiency Fully CMOS VCO Rectifier for Microwatt Resonant Wireless Power Transfer," IEEE Transactions on Circuits and Systems II: Express Briefs, vol.62, no.2, pp.134-138, Feb. 2015.
- [7] K. Colak, E. Asa, M. Bojarski, D. Czarkowski, "A Novel Multi-Level Phase-Controlled Resonant Inverter with Common Mode Capacitor for Wireless EV Chargers," IEEE International Conference on Transportation Electrification (ITEC), pp.1-6, Jun. 2015.
- [8] A. Namadmalan, "Bidirectional Current-Fed Resonant Inverter for Contactless Energy Transfer Systems," IEEE Transactions on Industrial Electronics, vol.62, no.1, pp.238-245, Jan. 2015.
- [9] O. Lazaro, G. A. Rincon-Mora, "A Nonresonant Self-Synchronizing Inductively Coupled 0.18- $\mu$ m CMOS Power Receiver and Charger," IEEE Journal of Emerging and Selected Topics in Power Electronics, vol.3, no.1, pp.261-271, Mar. 2015.
- [10] M. Bojarski, E. Asa, D. Czarkowski, "Effect of Wireless Power Link Load Resistance on the Efficiency of the Energy Transfer," IEEE International Electric Vehicle Conference (IEVC), pp.1-7, Dec. 2014.
- [11] R. P. Twiname, D. J. Thrimawithana, U. Madawala, C. A. Baguley, "A Dual Active Bridge Topology with a Tuned CLC Network," IEEE Transactions on Power Electronics, Early Access, DOI: 10.1109/TPEL.2014.2384511.
- [12] B. Nguyen, D. Vilathgamuwa, G. Foo, P. Wang, A. Ong, U. Madawala, T. Nguyen, "An Efficiency Optimization Scheme for Bidirectional Inductive Power Transfer Systems," IEEE Transactions on Power Electronics, vol.30, no.11, pp.6310-6319, Nov. 2015.
- [13] U. K. Madawala, M. Neath, D. J. Thrimawithana, "A Power Frequency Controller for Bidirectional Inductive Power Transfer Systems," IEEE Transactions on Industrial Electronics, vol.60, no.1, pp.310-317, Jan. 2013.
- [14] D. J. Thrimawithana, U. K. Madawala, M. Neath, "A Synchronization Technique for Bidirectional IPT Systems," IEEE Transactions on Industrial Electronics, vol.60, no.1, pp.301-309, Jan. 2013.
- [15] D. J. Thrimawithana, U. K. Madawala, "A Generalized Steady-State Model for Bidirectional IPT Systems," IEEE Transactions on Power Electronics, vol.28, no.10, pp.4681-4689, Oct. 2013.
- [16] U. K. Madawala, D. J. Thrimawithana, "Modular-based inductive power transfer system for high-power applications," IET Power Electronics, vol.5, no.7, pp.1119-1126, Aug. 2012.
- [17] M. J. Neath, A. K. Swain, U. K. Madawala, D. J. Thrimawithana, "An Optimal PID Controller for a Bidirectional Inductive Power Transfer System Using Multiobjective Genetic Algorithm," IEEE Transactions on Power Electronics, vol.29, no.3, pp.1523-1531, Mar. 2014.
- [18] A. K. Swain, S. Devarakonda, U. K. Madawala, "Modeling, Sensitivity Analysis, and Controller Synthesis of Multipickup Bidirectional Inductive Power Transfer Systems," IEEE Transactions on Industrial Informatics, vol.10, no.2, pp.1372-1380, May 2014.
- [19] U. K. Madawala, D. J. Thrimawithana, "Current Sourced Bi-directional Inductive Power Transfer System," IET Power Electronics, vol.4, no.4, pp.471-480, Apr. 2011.
- [20] U. K. Madawala, D. J. Thrimawithana, "A Bidirectional Inductive Power Interface for Electric Vehicles in V2G Systems," IEEE Transactions on Industrial Electronics, vol.58, no.10, pp.4789-4796, Oct. 2011.